compounds

MDPI

Article

Synthesis and Optical Properties of Red Carbon@$(NH_4)_3ZnCl_5$ Hybrid Heterostructures

Walker Vinícius Ferreira do Carmo Batista [1], Aniely Pereira de Souza [1], Tais dos Santos Cruz [1], Dilton Martins Pimentel [1], Danila Graziele Silva de Avelar [1], Sarah Karoline Natalino Oliveira [1], Wanessa Lima de Oliveira [2], Danilo Roberto Carvalho Ferreira [2], Márcio Cesar Pereira [3], Rondinele Alberto dos Reis Ferreira [4] and João Paulo de Mesquita [1,*]

[1] Department of Chemistry, Universidade Federal dos Vales do Jequitinhonha e Mucuri, Diamantina 39100-000, MG, Brazil; walker.vinicius@ufvjm.edu.br (W.V.F.d.C.B.); aniely.souza@ufvjm.edu.br (A.P.d.S.); tais.cruz@ufvjm.edu.br (T.d.S.C.); dilton.pimentel@ufvjm.edu.br (D.M.P.); danila.avelar@ufvjm.edu.br (D.G.S.d.A.); sarah.karoline@ufvjm.edu.br (S.K.N.O.)
[2] Nuclear Technology Development Center, Belo Horizonte 31270-901, MG, Brazil; wanessa.oliveira@ufvjm.edu.br (W.L.d.O.); danilo.ferreira@cdtn.br (D.R.C.F.)
[3] Institute of Science, Engineering and Technology, Universidade Federal dos Vales do Jequitinhonha e Mucuri, Teófilo Otoni 39803-371, MG, Brazil; marcio.pereira@ufvjm.edu.br
[4] Faculty of Chemical Engineering, Universidade Federal de Uberlândia, Uberlândia 38408-100, MG, Brazil; rondinelealberto@gmail.com
* Correspondence: joao.mesquita@ufvjm.edu.br

Abstract: In this study, we report the synthesis and characterization of hybrid heterostructures composed of red carbon, an organic semiconductor polymer, and the perovskite $(NH_4)_3ZnCl_5$. Red carbon was synthesized via the polymerization of carbon suboxide (C_3O_2), exhibiting strong light absorption and distinctive optical properties. The hybrid material was obtained by crystallizing $(NH_4)_3ZnCl_5$ in the presence of red carbon, leading to significant modifications in the optical characteristics of the perovskite. Comprehensive analyses, including X-ray diffraction, FTIR spectroscopy, UV-vis spectroscopy, and cyclic voltammetry, confirmed the formation of a type I heterostructure with enhanced luminescence and potential for advanced optical applications. The energy band alignment suggests that red carbon can function effectively as both a hole and electron transport medium. This work underscores the potential of $(NH_4)_3ZnCl_5$@red carbon hybrid heterostructures in the development of next-generation optoelectronic devices, including sensors and LEDs.

Keywords: perovskite; suboxide; red carbon; heterostructure; optical properties

check for updates

Academic Editor: Philippopoulos Athanassios

Received: 28 March 2025
Revised: 20 May 2025
Accepted: 4 June 2025
Published: 10 June 2025

Citation: Batista, W.V.F.d.C.; de Souza, A.P.; Cruz, T.d.S.; Pimentel, D.M.; de Avelar, D.G.S.; Oliveira, S.K.N.; de Oliveira, W.L.; Ferreira, D.R.C.; Pereira, M.C.; Ferreira, R.A.d.R.; et al. Synthesis and Optical Properties of Red Carbon@$(NH_4)_3ZnCl_5$ Hybrid Heterostructures. *Compounds* **2025**, *5*, 21. https://doi.org/10.3390/compounds5020021

Copyright: © 2025 by the authors. Licensee MDPI, Basel, Switzerland. This article is an open access article distributed under the terms and conditions of the Creative Commons Attribution (CC BY) license (https://creativecommons.org/licenses/by/4.0/).

1. Introduction

In the last decade, ternary compounds based on the perovskite structure have attracted great attention from the scientific community, especially because of the power conversion efficiency (PCE) [1]. However, perovskite halides have been considered for several other applications becoming a prominent field of research in recent years because of their distinct photo-physical features that include a tunable band-gap, long diffusion length, and high carrier mobility [2,3]. Despite their fantastic photoelectric properties, several strategies have been used to improve their performance and expand their field of application. The development of heterostructures with a wide range of materials has been considered to have positive impacts on the properties and performance of devices based on metal halide perovskites [3–6]. In this context, hybrid heterostructures of metal halide perovskites using carbon-based materials

(graphene, carbon dots) [7,8] and organic semiconductors have received increasing attention because of their unique optical and electrical characteristics [9–11].

Metal halide perovskite-based optoelectronics has experienced an unprecedented development in the last decade, while further improvements in the efficiency, stability, and economic gains of such devices require novel engineering concepts. The use of carbon nanoparticles as versatile auxiliary components of perovskite-based optoelectronic devices is one strategy that offers several advantages in this respect.

On the one hand, the development of hybrid heterostructures based on halide perovskites is an interesting and viable strategy to improve the properties of optoelectronic energy devices [12], sensors [8], and photocatalysis [3]; on the other hand, it can contribute to a better understanding of the physical–chemical processes involved at the interface between the compounds and strategies for the protection of the structure and surface of perovskite-based material, motivating the synthesis and future development of new and more efficient halide perovskite-based heterostructures [6,7,13,14].

Here, we report, for the first time, a study on forming a hybrid heterostructure among a metal halide perovskite, $(NH_4)_3ZnCl_5$, and an organic semiconductor called "red carbon". The $(NH_4)_3ZnCl_5$ crystallizes in the orthorhombic *Pnma* space group. In general, A_3BX_5-based perovskite structures have been much less explored compared to the widely studied ABX_3 counterparts, although A_3BX_5-based materials will demonstrate superior properties for photonic applications [15].

Red carbon is a conjugated organic polymer/oligomer with semiconductor properties derived from carbon suboxide (C_3O_2) [16]. Carbon suboxide and other "oxycarbons" were first reported in 1873 by Brodie, during research on the effect of an electric current on carbon monoxide [17]. Currently, this structure is obtained mainly from the dehydration of malonic acid [16,18,19]. A solid state investigation using single-crystal X-ray diffraction revealed that the crystal belongs to the *Pnma* space group, being constituted by two non-crystallographically equivalent molecules in the asymmetric unit: a = 986.9(2), b = 1206.0(2), c = 516.0(1) pm [18]. It presents a conjugated molecular structure formed of pyrone units with a band gap of ~1.9 eV, high molar absorptivity, and good ability to form films [16,20]. The small band gap and the positions of their valence and conduction bands are suitable for the formation of both type I and type II heterostructures with both metal halide perovskites that are activated by visible light and those with a band gap in the ultraviolet region of the electromagnetic spectrum [21]. In addition to the different optical and electronic properties, the "carbon networks" present a significant and homogeneous concentration of oxygenated functional groups that can contribute to the formation of heterostructures such as perovskites. Furthermore, the synthesis of carbon-based materials with a homogeneous and controllable molecular chemical structure is essential for the elucidation of reaction mechanisms in different applications [22,23].

Despite its interesting properties, it feels manageable and easy, but the work in the literature on red carbon is still very rarely reported [24,25]. Odziomek et al. investigated the photocatalytic properties of carbon red in the oxidation of thioanisole and benzyl alcohol. On the one hand, if the oxidation of sulfurous compost was not very selective, the oxidation of alcohol resulted in a 74% yield of benzaldehyde [16]. Ba et al. used red carbon as a precursor for the preparation of an oxocarbon framework containing dispersed Cu_2O clusters. The new material was tested for the electroreduction of nitrate under acidic conditions and presented a high yield rate of ammonium (NH_4^+) at 3.31 mmol h^{-1} $mgcat^{-1}$ with a Faradaic efficiency of 92.5% at −0.4 V (vs RHE) [24]. Giusto et al. reported the use of the material for the preparation of thin films and its use as a platform for amine sensing [20].

Since one of the main challenges associated with the preparation of heterostructures based on perovskite-type materials is the establishment of heterojunctions, here, we pro-

pose, for the first time, the use of red carbon in the preparation of hybrid heterostructures with $(NH4)_3ZnCl_5$ structures. We explore the impact of red carbon on a perovskite that does not absorb in the visible region of the electromagnetic spectrum, thus being less suitable for photovoltaic applications [26].

2. Materials and Methods

2.1. Chemical Reagents

Hydrochloric acid 38%, ammonium chloride 99.5%, and zinc chloride 96% were provided by Êxodo Científica (Sumaré, Brazil). Malonic acid 98% was obtained from ACS Cientifica (Sumaré, Brazil). Acetic anhydride 97% was obtained from Dinâmica (Indaiatuba, Brazil), ethyl alcohol 99.5% was obtained from Vetec, and isopropyl alcohol 99.8% were obtained from Exodo (Sumaré, Brazil). All chemicals were used directly without further purification.

2.2. Preparation of the Materials

2.2.1. Preparation of Red Carbon

Red carbon was prepared according to the procedure published elsewhere [16]. Briefly, 10 g of malonic acid was mixed with 19.6 g of acetic anhydride in a glass round-bottom flask. The mixture was heated to 90 °C to dissolve the malonic acid, and then, the temperature was raised to 140 °C. The reaction was carried out under these conditions for 5 h. During this time, changes in color and viscosity of the system could be visually observed, changing from a clear solution to a yellow solution and finally a very dark suspension. The resulting material was filtered and washed with ethyl ether and then dried in an oven at 90 °C.

2.2.2. Preparation of $(NH_4)_3ZnCl_5$ Perovskites and Heterostructure

The perovskite $(NH_4)_3ZnCl_5$ was synthesized in a hydrochloric acid solution. Briefly, 1.36 g of zinc (II) chloride was dissolved in 1 mL of 1 M hydrochloric acid, and 0.80 g of ammonium chloride was dissolved in 3 mL of hydrochloric acid (1 M) together with 0.5 mL of isopropyl alcohol. The solutions were combined and heated at 80 °C until the solvent volume was reduced to 2 mL, during which a color change from clear to yellowish was observed. The solution was then placed in an ice bath until crystals formed. The crystals were filtered using a sintered glass funnel, washed with isopropyl alcohol and ether, and then transferred to a Petri dish to be dried in desiccators for 24 h. The red carbon@$(NH_4)_3ZnCl_5$ heterostructures were prepared following the synthesis methodology for $(NH_4)_3ZnCl_5$ with the addition of 2% red carbon.

2.3. Characterizations

FTIR spectra were obtained with an IRSPIRIT spectrometer (Shimadzu, Kyoto, Japan) using an ATR module (QATR-S). X-ray diffraction (XRD) data were obtained with a Shimadzu diffractometer (XRD6000) to evaluate changes in the crystal structure after alkaline exfoliation. Rietveld refinement was performed to determine the crystal structure from X-ray diffraction data, from which it was possible to obtain detailed structural parameters and quantification of the crystalline phases present in the sample. All adjustments were conducted using *FullProf* software, version 2023. The morphology of the samples was observed using a Tescan (Brno, Czechia) scanning electron microscope (model VEGA3 LMH). Energy-dispersive X-ray Spectroscopy (EDS), coupled to a microscope, was used for elemental composition and mapping. Reflectance diffuse data were obtained using a spectrometer UV-Vis Varian Cary 50 using a Diffuse-Reflection Accessory DiffusIR (PIKE). Stationary fluorescence analyses were performed on a PerkinElmer (Waltham, MA, USA)

EnSpire spectrofluorometer with a slit width of 10 nm, using a Brandplates-pureGrade white flat-bottom plate with 96 wells.

The cyclic voltammograms were obtained with a Metrohm Autolab PGSTAT 128N potentiostat/galvanotate (Herisau, Switzerland) at room temperature using a conventional three electrode arrangement with a Pt wire counter electrode and a saturated Ag/AgCl reference electrode. The glass carbon (Ø 0.9 mm) was used as a working electrode. The electrochemical measurements were obtained for a 0.01 $mgmL^{-1}$ red carbon solution within a potential window of −1.4 and 2.0 V with a scan speed of 50 mVs^{-1}. A 0.1 M $MgClO_4$ (Aldrich, St. Louis, MO, USA) solution prepared in acetonitrile was used to support the electrolyte, previously purged with nitrogen for 15 min. For the electrochemical characterization of the perovskite-based material, a paste was prepared combining the solid and magnesium perchlorate solution. The mixture was stirred until a homogeneous consistency was achieved and then applied to the surface of a glassy carbon electrode, which had been previously cleaned with alumina and dried with nitrogen gas. Cyclic voltammetry was performed at a scan rate of 50 mV/s, with a potential range from −2 V to 2 V. Based on work published elsewhere [7,27], the energy level relative to the vacuum level for the valence and conduction bands was determined using Equations (1) and (2)

$$E_{VB} = -e(E_{\mathrm{Ox}} + 4.64) \quad (1)$$

$$E_{CB} = E_{VB} + E_{BG} \quad (2)$$

where E_{VB} is the valence band energy, E_{CB} is the conduction band energy, and E_{Ox} is the onset of oxidation potential. E_{BG} is the electrochemical or optical band-gap. The optical band gap was estimated using a Tauc plot.

3. Results

Figure 1 shows the synthetic route used in the preparation of the materials studied in this work.

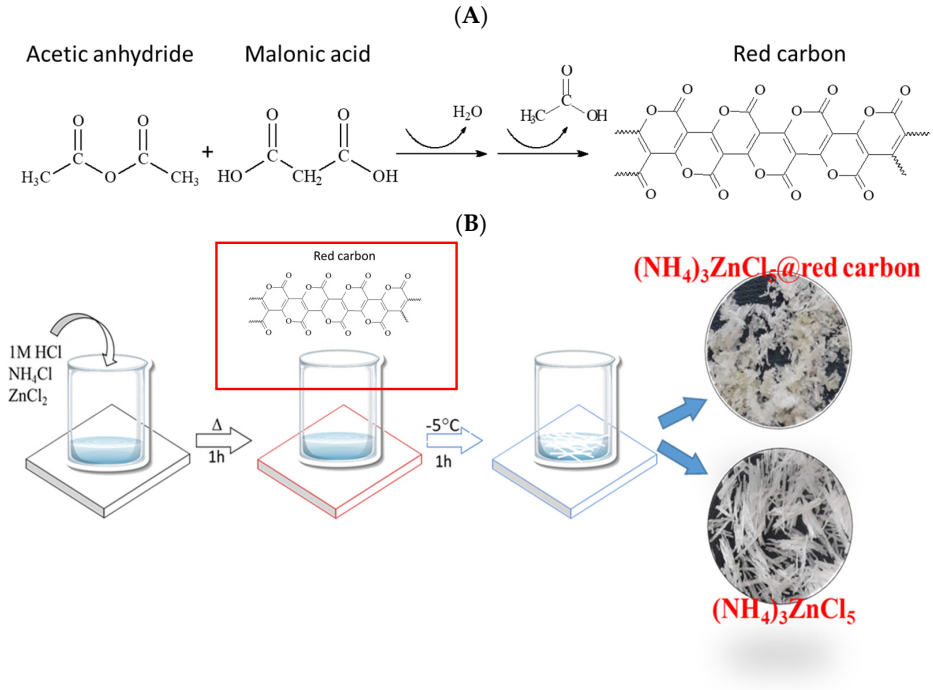


Figure 1. (**A**) Simplified reaction mechanism based on activation of malonic acid by acetic anhydride for obtained red carbon. (**B**) Schematic illustration of the steps to obtain $(NH_4)_3ZnCl_5$ and $(NH_4)_3ZnCl_5$@red carbon.

3.1. Red Carbon Characterization

Red carbon is formed from the polymerization of carbon suboxide (C_3O_2) in a relatively simple procedure, recently developed by Odziomek et al. [16]. In this alternative procedure to the use P_2O_5, the dehydration of malonic acid is carried out using acetic anhydride (Figure 1A). During the reaction, acetic anhydride reacts with a molecule of malonic acid, releasing water molecules (dehydration) to form an intermediate structure containing four carbonyls. The suboxide carbon monomer is then formed from a structural rearrangement of this intermediate by releasing two molecules of acetic acid for each monomer unit (C_3O_2), which polymerizes spontaneously into highly conjugated light-absorbing structures [16]. Figure S1 shows digital images of red carbon suspensions (0.06 mgmL^{-1}) in different solvents under ambient and UV light.

Figure 2A shows the X-ray diffractogram obtained for the product of the reaction between malonic acid and acetic anhydride. The diffraction pattern obtained for the precursor malonic acid is shown in Figure S2. The observed profile presents three regions of intense diffractions, centered respectively at 19.5, 25.1 and 33.2 2θ. The diffraction peak observed at 44.1 2θ originates from the diffraction of the aluminum sample holder. The peak at 25.1 2θ, corresponding to an interplanar distance of 3.5 Å, is attributed to the spacing of the polypyrrone chains, with the shoulder observed at 22.9 2θ, possibly due to the presence of structures with different degrees of crystallinity. The other diffraction peaks are associated with the interplanar distances of the molecular structures that form the polymer chains of the semiconductor.

The FTIR spectrum shown in Figure 2B presents the characteristic absorption bands of the functional groups present in the polymeric structure of red carbon. The presence of cyclic esters is confirmed by the band centered at 1736 cm^{-1}, characteristic of the C=O stretching, in addition to the absorptions observed at 1170 and 1130 cm^{-1}, characteristic of C-O stretching. The presence of C=C bonds is confirmed by the absorption at 1611 cm^{-1} and 1520 cm^{-1}. Although the intense absorption of the band centered at 796 cm^{-1} is still little discussed, with some authors attributing it to the presence of ether-like functional groups at the edges of graphene structures [3,8], we believe that the absorption is associated with the vibrations of the pyrone-like units, which form the polymeric structure of the material, similarly to the triazine rings observed in graphitic carbon nitrides.

Figure 2C shows the image of red carbon in a solid state and its dispersion in acetonitrile. Under ambient light, the red carbon solution in acetonitrile appears reddish-yellow in color, while under UV light (λ_{max} = 360 nm), the solution exhibits strong emission in the green region of the electromagnetic spectrum (inset in Figure 2C). On the other hand, in water and DMF, the red carbon dispersion emits in the blue and yellow regions, respectively (Figure S1).

The UV-Vis spectrum of the red carbon obtained by diffuse reflectance of the solid sample presents an optical maximum absorption around the 400 nm region that extends to ~700 nm. On the other hand, the spectrum of the sample in acetonitrile shows an absorption starting at 600 nm. The bathochromic shift observed in the spectrum of the solid sample has been attributed to the presence of intermolecular interactions of the material's oligomeric structures [16].

According to the molecular structure, the polymer presents two main chromophores, C=C (π-π transitions) and C=O (π-π and n-π transitions), in a broad conjugated system, which justifies its high absorption in the visible region of the spectrum (Figure 2D). Due to the characteristics of the π-π transitions that are allowed (unlike the n-π, which are forbidden by symmetry) [28], therefore being more intense and that undergo a more accentuated bathochromic shift, the spectrum does not present these band distinctions. From the TAUC plot, the band gap was estimated at 1.95 eV (Figure S3).

The electronic band structure of the material was investigated using cyclic voltammetry. Figure 3 shows a typical cyclic voltammogram obtained for the red carbon solution with a scan rate of 50 mVs^{-1}. The voltammogram shows the presence of well-defined redox peaks at 1.54 V and −0.70 V corresponding to the oxidation and reduction processes of the material structure, respectively. The onsets of oxidation (EOx) and reduction (ERed) potentials were estimated at 1.34 and −0.29 V, which corresponds to an electrochemical band gap of ~1.63 eV. From these results, the energy relative to the vacuum level of the top of the valence band and bottom of the conduction band was estimated at −5.98 and −4.35 eV, respectively.

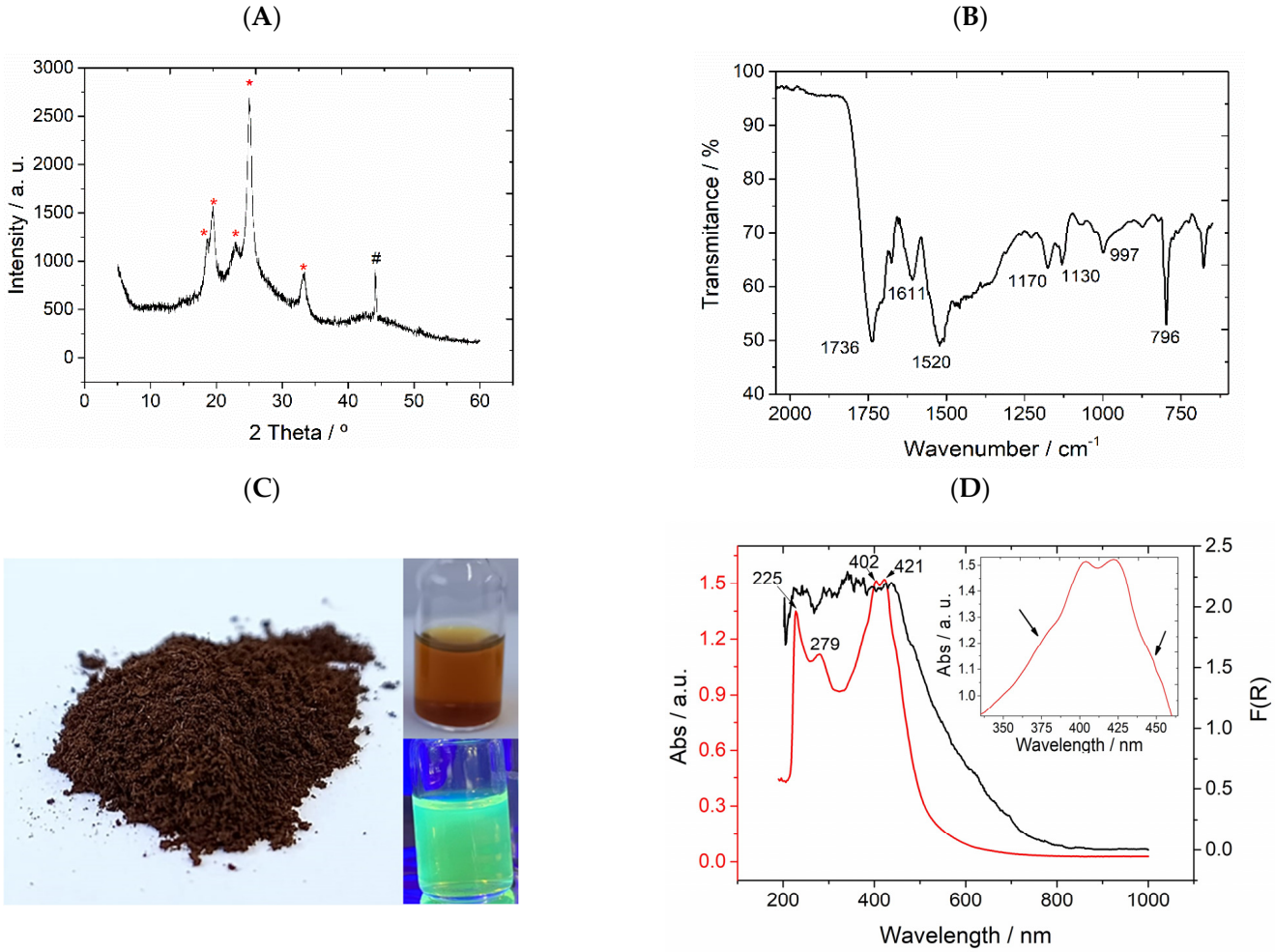


Figure 2. (**A**) XRD pattern and (**B**) FTIR spectra obtained for red carbon. (**C**) Image of the material in powder form and in acetonitrile solution under ambient light (top) and exposed to a UV lamp (bottom). (**D**) UV-Vis spectrum obtained for the solid material and in an acetonitrile solution (0.06 $mgmL^{-1}$). Inset: magnification of the region located between 340 and 460 nm of the spectrum obtained for the solution.

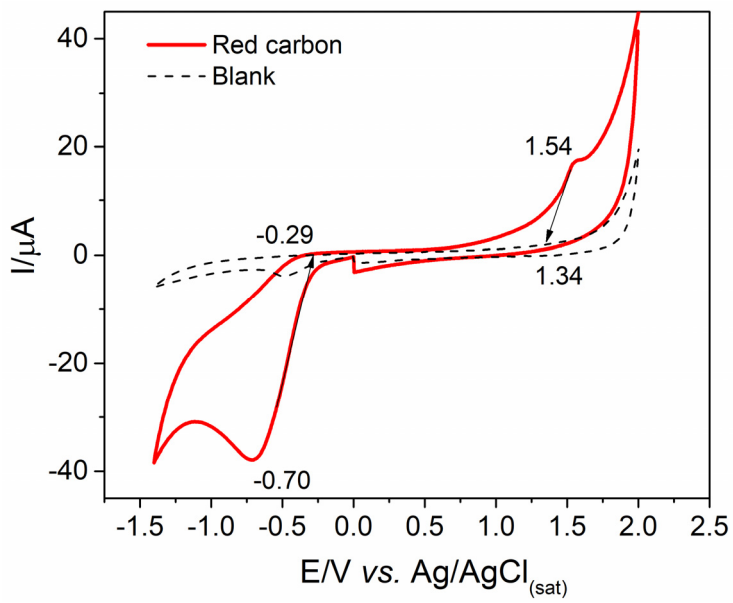


Figure 3. Cyclic voltammogram obtained for a solution of 0.01 mgmL^{-1} of "red carbon" dispersed in a supporting electrolyte of 0.1 M magnesium perchlorate/acetonitrile. The scan started at 0 V in the cathodic direction with a scan speed of 50 mVs^{-1}.

3.2. Characterization of $(NH_4)_3ZnCl_5$ Perovskite@Red Carbon Heterostructures

Figure 4A,B show the crystallization products of solutions containing NH_4Cl and $ZnCl_2$ in the absence and presence of red carbon. In the absence of organic structures, the formation of crystals with a well-defined needle-like morphology of millimeters in length is observed. On the other hand, the crystallization of the perovskite halide in the presence of red carbon does not present a well-defined pattern indicating the interaction of the organic semiconductor with the ternary phase during the crystallization process, which is confirmed by the yellowish coloration of the crystals to the detriment of the translucent needles observed for the pure crystals.

The yellowish coloration can be better verified in Figure S4, which shows images of the suspensions of both materials in acetonitrile after two minutes in an ultrasound bath.

The X-ray diffractogram is consistent with the crystalline phase $(NH_4)_3ZnCl_5$ (Card number 30–69). The Rietveld refinement results revealed significant information about the composition of the sample prepared with NH_4Cl and $ZnCl_2$. The diffraction patterns obtained for these precursor reagents are shown in Figure S2. The qualitative analysis performed with the Search-Match 2.0.2.0 and X'Pert HighScore Plus 3.0 software indicated the presence of the $(NH_4)_2ZnCl_4$ and $(NH_4)_3ZnCl_5$ phases. These results highlight that $(NH_4)_3ZnCl_5$ is the predominant phase, while $(NH_4)_2ZnCl_4$ is only a residual byproduct. The predominance of $(NH_4)_3ZnCl_5$ suggests that the experimental conditions, such as temperature and concentration of the reagents, favored the formation of this main phase over the other observed phase. The X-ray diffraction pattern obtained for the $(NH_4)_3ZnCl_5$ sample attests to the excellent crystallinity of this material. The Rietveld method reveals a structure indexed in an ortorrombic lattice (Pnma space group) with lattice parameters a = 7.21 Å, b = 12.74(4) Å, c = 9.28 Å, and $\alpha = \beta = \gamma = 90°$ [29]. $(NH_4)_3ZnCl_5$ crystallizes in an orthorhombic system (space group Pnma) and is isostructural with various A_3BX_5-type halides, such as $(NH_4)_3ZnBr_5$ and $CsZnI_5$. Its structure features isolated $[ZnCl_4]^{2-}$ tetrahedra and additional chloride ions, with NH_4^+ ions occupying interstitial sites and stabilizing the framework via hydrogen bonding. The Zn^{2+} center is tetrahedrally coordinated by Cl^- ions. This structural arrangement is distinct from tetragonal variants like Cs_3CoCl_5. The compound forms preferentially in ammonium-chloride-rich conditions, and X-ray

diffraction is used to distinguish it from similar phases. Intermediate stoichiometries may yield mixed phases containing both $(NH_4)_2ZnCl_4$ and $(NH_4)_3ZnCl_5$ [30,31].

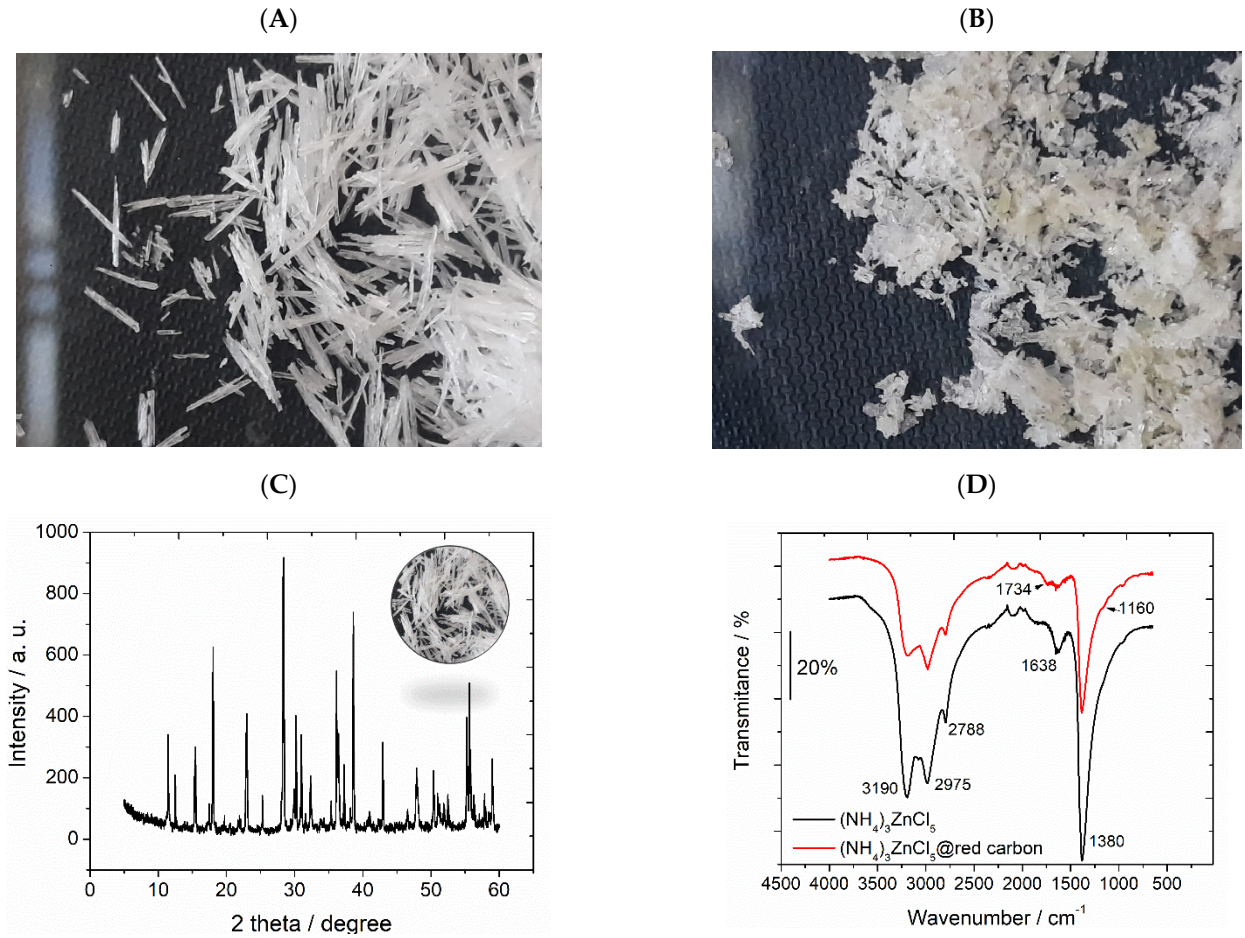


Figure 4. Digital images of $(NH_4)_3ZnCl_5$ crystals in the absence (**A**) and presence (**B**) of red carbon. (**C**) XRD pattern with Rietveld refinements and (**D**) FTIR spectra obtained for potassium $(NH_4)_3ZnCl_5$ and $(NH_4)_3ZnCl_5$@red carbon.

To examine the ratios of the elements, energy dispersive spectroscopy (EDS) analyses were carried out on a single crystal, and the results obtained (see Supplementary Information, Figure S5, Table S1) are consistent with the stoichiometric ratio of the compound $(NH_4)_3ZnCl_5$, which presents 18, 22, and 60 wt% for NH_4^+, Zn, and Cl, respectively.

EDS element-mapping was performed to prove the uniformity of the bulk crystalline of $(NH_4)_3ZnCl_5$ and confirm the presence of the organic structures in the material composition of $(NH_4)_3ZnCl_5$@red carbon (Figure 5).

The FTIR analysis obtained for $(NH_4)_3ZnCl_5$ crystals is typical of this crystalline phase with the presence of stretching and deformation bands of the ammonium ion at 3190, 2975, 2788, and 1380 cm^{-1} [32]. The spectrum of the sample crystallized in the presence of red carbon is predominantly of the $(NH_4)_3ZnCl_5$ structure, but the bands at 1160 and principally at 1734 cm^{-1} confirm the presence of the polymeric semiconductor associated with the perovskite structure.

The optical properties of the $(NH_4)_3ZnCl_5$ and $(NH_4)_3ZnCl_5$@red carbon were investigated via UV–vis spectroscopy. Figure 6 shows the electronic spectra obtained for these materials. For the $(NH_4)_3ZnCl_5$ sample, absorption begins at 400 nm with a direct band gap, estimated from the Tauc plot, of 3.6 eV. On the other hand, in the composite material, absorption begins at 700 nm, with a strong intensity from 500 nm with a maximum at approximately 386 nm. This result is similar to that observed for red carbon, but with small

shifts in wavelengths due to the interaction with the $(NH_4)_3ZnCl_5$ structure. The band gap was estimated at 2.7 eV. The intermediate value between 1.95 to 3.6 eV, observed in the composite band structure coupling, enabling electron excitation from the valence band of one material to the conduction band of the other.

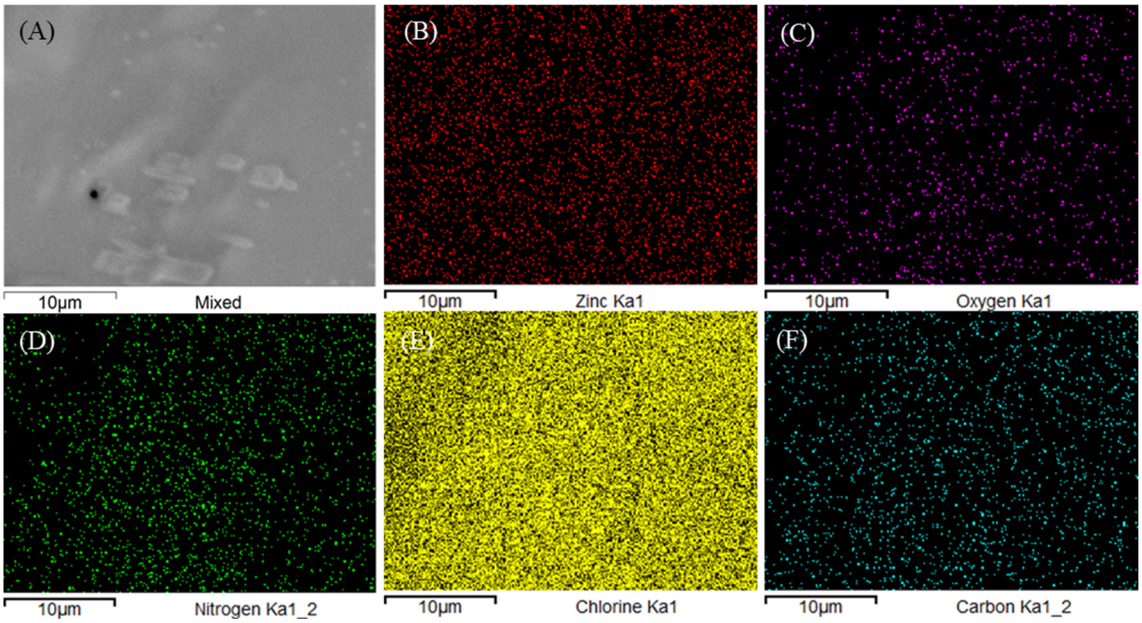


Figure 5. EDS element-mapping images of $(NH_4)_3ZnCl_5$@red carbon. (**A**) SEM image, (**B**–**F**) elemental distributions, zinc (red), oxygen (violet), nitrogen (green), chlorine (yellow), and carbon (cyan).

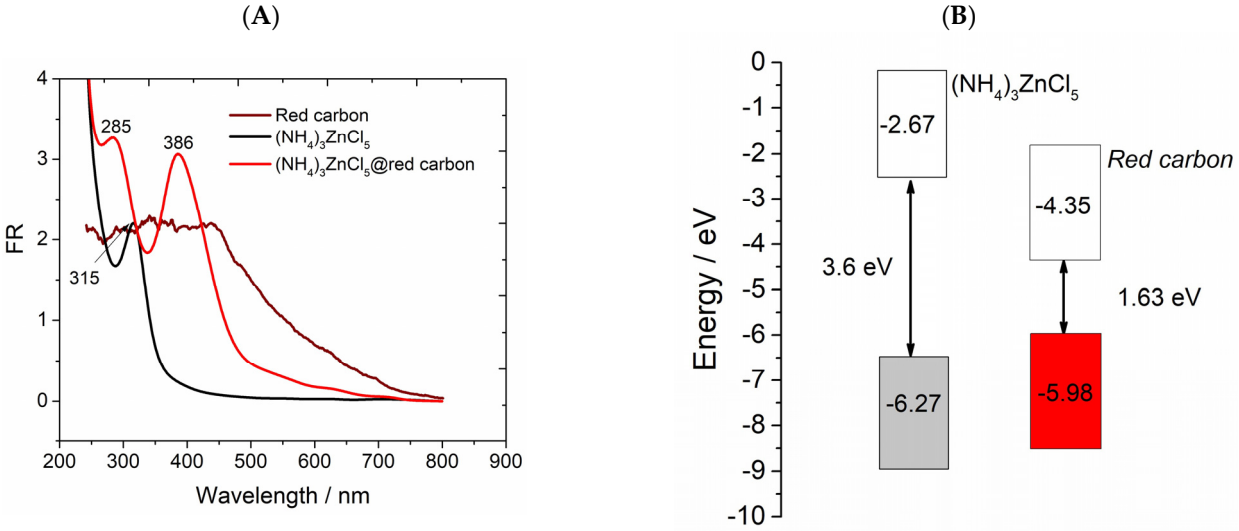


Figure 6. (**A**) UV–Vis spectra obtained for $(NH_4)_3ZnCl_5$ and red carbon@$(NH_4)_3ZnCl_5$. The absorbance values were obtained using the Kubelka–Munk function from the normalized reflectance data. (**B**) Valence band top and conduction band bottom energies estimated for $(NH_4)_3ZnCl_5$ and red carbon from electrochemical UV-Vis spectroscopy measurements.

From Equations (1) and (2), the band structure of $(NH_4)_3ZnCl_5$ was determined. The energy of the conduction band top was estimated to be −2.57, while the valence band bottom was calculated to be −6.17 eV (Figure S6). According to the energy band alignments of the semiconductors involved, the inorganic semiconductor $(NH_4)_3ZnCl_5$, and the organic semiconductor red carbon, the results indicate the formation of a type I heterostructure, in which the conduction band bottom (CB) and valence band bottom (VB) of the inorganic semiconductor are larger and smaller, respectively, than those observed

for the organic semiconductor, which presents a narrow band gap (Figure 6B). Type I heterojunctions, both holes and electrons generated in semiconductor A $(NH_4)_3ZnCl_5$ will move to semiconductor B (red carbon). Then, it can recombine within semiconductor B or at the interface, effectively improving the luminescence properties and performance [33].

The photoluminescence spectra obtained for the samples studied are shown in Figure 7. The photoluminescence spectrum of the $(NH_4)_3ZnCl_5$ sample shows the presence of two peaks, one more intense at 435 nm (2.85 eV) and another with lower intensity at 495 nm (2.50 eV). The presence of two peaks for perovskite-based structures has been associated with different factors including the presence of two components [34], coexistence of radiative direct and indirect transitions, strain-induced defects in the bulk, surface defect states, and optical effects caused from an extensive self-absorption effect [35] and is normally observed in quasi-2D structures [36]. For red carbon, as observed for other carbon nanostructures, for example, carbon dots, the different emission peaks may be associated with differences in sizes, crystallinity, and compositions of the structures that make up the sample or even surface defects. In the spectrum of the composite material (red carbon@$(NH_4)_3ZnCl_5$), a significant increase in the intensity of the emissions is observed. The increase in intensity corroborates the interpretation regarding the formation of a type I heterostructure. It is also possible to observe a significant broadening of the emission bands, especially in the band located in the visible region of the electromagnetic spectrum, with a significant increase in emission at wavelengths greater than 500 nm. In the nominalized spectrum (Figure 7B) of the heterostructure, an inversion of the relative intensities between peaks centered at 439 and 496 nm is also observed due to the contribution of the emission originating in the red carbon structure.

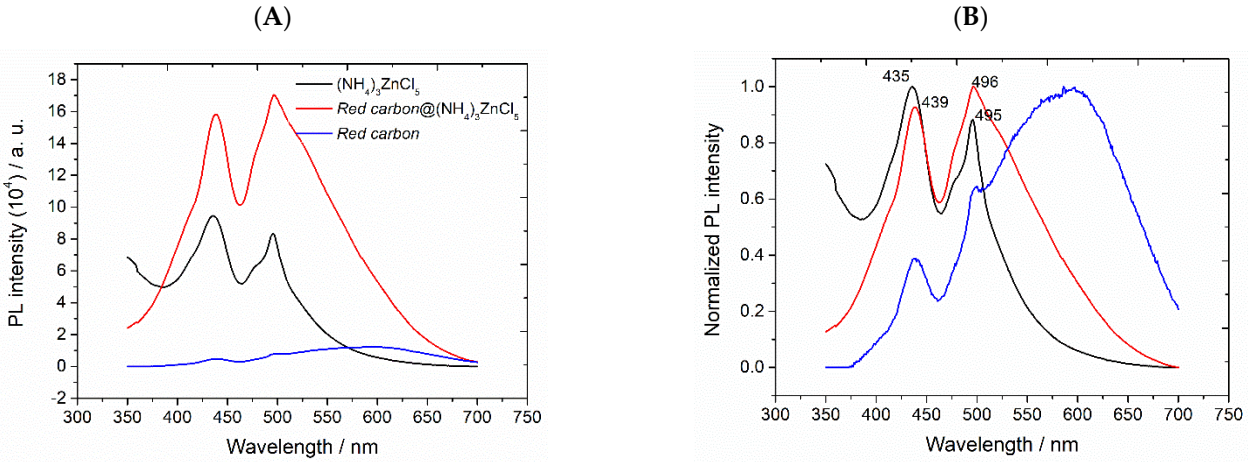


Figure 7. (**A**) Photoluminescence spectra obtained for $(NH_4)_3ZnCl_5$, red carbon@$(NH_4)_3ZnCl_5$, and red carbon with a 250 nm excitation. (**B**) Normalized results.

Finally, in addition to the structural and optical characterization presented, the red carbon@$(NH_4)_3ZnCl_5$ hybrid heterostructure demonstrates properties that make it a promising candidate for practical applications, such as environmental monitoring, food quality control, and biomedical diagnostics. The formation of a type I heterojunction and the observed enhancement in photoluminescence suggest strong potential for the development of optoelectronic devices—particularly sensors that rely on changes in the electrochemical or optical response of the material upon interaction with target analytes.

4. Conclusions

The $(NH_4)_3ZnCl_5$ structure was successfully crystallized in the presence of red carbon, a semiconductor organic polymer derived from the suboxide molecule (C_3O_2). The red

carbon was characterized using different techniques, and its band structure was determined from cyclic voltammetry measurements in an organic electrolyte support. On the other hand, the obtained composite presented significant changes in optical properties with a red shift in absorption and a significant increase in emissions in the visible region of the electromagnetic spectrum due to the formation of a type I heterostructure, which has potential applications in the development of different optical devices. Considering the energies of the conduction band bottom (CB) and valence band bottom (VB), red carbon could also be considered an alternative for transporting holes for traditional hybrid metal halide structures in the development of optoelectronic devices. Thus, the incorporation of red carbon represents a promising strategy for the improvement and development of next-generation optoelectronic devices for a wide range of applications, including sensors and light-emitting devices.

Supplementary Materials: The following supporting information can be downloaded at: https://www.mdpi.com/article/10.3390/compounds5020021/s1, Figure S1: (A) Red carbon powder. (B) Digital images of red carbon suspensions (0.06 $mgmL^{-1}$) in different solvents under ambient (B) and UV light (C), Figure S2: X-ray diffractograms obtained for the precursor reagents used in the synthesis of red carbon (malonic acid) and $(NH_4)_3ZnCl_5$ (zinc chloride, PDF card 39-887, and ammonium chloride, PDF card 7-7), Figure S3: The Tauc plots obtained for red carbon for the direct transition, Figure S4: Images of $(NH_4)_3ZnCl_5$ (white) $(NH_4)_3ZnCl_5$@red carbon (yellow) suspensions, Figure S5: Energy dispersive X-ray spectroscopy (EDS) spectra of $(NH_4)_3ZnCl_5$. The measured atomic percentages of the main elements (Zn, N, Cl) in the perovskite are summarized in Table S1, Figure S6: Cyclic voltammograms obtained for $(NH_4)_3ZnCl_5$ anchored on a surface glass carbon electrode in a supporting electrolyte of 0.1 M magnesium perchlorate/acetonitrile; Table S1: EDS elemental analysis of the $(NH_4)_3ZnCl_5$ sample.

Author Contributions: Methodology, W.V.F.d.C.B., A.P.d.S., T.d.S.C., D.M.P., D.G.S.d.A., W.L.d.O., D.R.C.F., M.C.P. and R.A.d.R.F.; Formal analysis, W.V.F.d.C.B., T.d.S.C., W.L.d.O. and D.R.C.F.; Investigation, W.V.F.d.C.B., A.P.d.S., T.d.S.C., D.M.P., S.K.N.O., W.L.d.O., D.R.C.F., M.C.P. and R.A.d.R.F.; Writing—original draft, D.M.P., D.G.S.d.A., S.K.N.O., W.L.d.O., M.C.P. and J.P.d.M.; Supervision, J.P.d.M.; Funding acquisition, J.P.d.M. All authors have read and agreed to the published version of the manuscript.

Funding: This research was supported by the Coordenação de Aperfeiçoamento de Pessoal de Nível Superior (CAPES 001) and by FAPEMIG through grants APQ-02754-24 and APQ-02629-17.

Institutional Review Board Statement: Not applicable.

Informed Consent Statement: Not applicable.

Data Availability Statement: The raw data supporting the conclusions of this article will be made available by the authors on request.

Acknowledgments: J.P.d.M. acknowledge grants from Conselho Nacional de Desenvolvimento Científico e Tecnológico (CNPq, 102190/2022-4). The authors gratefully acknowledge UFVJM for institutional support and the technical assistance provided by MULTIFART and LMMA through the FAPEMIG projects APQ-00370-22 and APQ-003088-21.

Conflicts of Interest: The authors declare no conflict of interest.

References

1. Kim, J.Y.; Lee, J.-W.; Jung, H.S.; Shin, H.; Park, N.-G. High-Efficiency Perovskite Solar Cells. *Chem. Rev.* **2020**, *120*, 7867–7918. [CrossRef]
2. Paul, T.; Hiralal Makani, N.; Sahoo, A.; Singh Tanwar, L.; Singh, M.; Banerjee, R. Halide perovskites for optoelectronic application. *Mater. Today Proc.* 2023; *in press*. [CrossRef]

3. Yuan, C.; He, Y.; Chen, R.; Sun, Y.; Li, J.; Cui, W.; Chen, P.; Sheng, J.; Dong, F. Perovskite Nanocrystals-Based Heterostructures: Synthesis Strategies, Interfacial Effects, and Photocatalytic Applications. *Sol. RRL* **2021**, *5*, 2000419. [CrossRef]
4. Shi, E.; Gao, Y.; Finkenauer, B.P.; Akriti; Coffey, A.H.; Dou, L. Two-dimensional halide perovskite nanomaterials and heterostructures. *Chem. Soc. Rev.* **2018**, *47*, 6046–6072. [CrossRef]
5. Bera, S.; Pradhan, N. Perovskite Nanocrystal Heterostructures: Synthesis, Optical Properties, and Applications. *ACS Energy Lett.* **2020**, *5*, 2858–2872. [CrossRef]
6. Hautzinger, M.P.; Raulerson, E.K.; Harvey, S.P.; Liu, T.; Duke, D.; Qin, X.; Scheidt, R.A.; Wieliczka, B.M.; Phillips, A.J.; Graham, K.R.; et al. Metal Halide Perovskite Heterostructures: Blocking Anion Diffusion with Single-Layer Graphene. *J. Am. Chem. Soc.* **2023**, *145*, 2052–2057. [CrossRef]
7. Ray, S.; Sahoo, M.R.; Mukherjee, S.; Perumal, A.; Nayak, S.K.; Bhaumik, S. Understanding the charge transfer mechanism in CsPbBr3 nanocrystals and nitrogen-doped carbon quantum dot heterostructures: Effect of nanocrystal encapsulation. *RSC Adv.* **2023**, *13*, 35551–35561. [CrossRef]
8. Algadi, H.; Ren, J.; Alqarni, A. A high-performance self-powered photodetector based on solution-processed nitrogen-doped graphene quantum dots/all-inorganic perovskite heterostructures. *Adv. Compos. Hybrid Mater.* **2023**, *6*, 98. [CrossRef]
9. Tyznik, C.; Lee, J.; Sorli, J.; Liu, X.; Holland, E.K.; Day, C.S.; Anthony, J.E.; Loo, Y.-L.; Vardeny, Z.V.; Jurchescu, O.D. Photocurrent in Metal-Halide Perovskite/Organic Semiconductor Heterostructures: Impact of Microstructure on Charge Generation Efficiency. *ACS Appl. Mater. Interfaces* **2021**, *13*, 10231–10238. [CrossRef]
10. Liu, C.-K.; Tai, Q.; Wang, N.; Tang, G.; Hu, Z.; Yan, F. Lead-Free Perovskite/Organic Semiconductor Vertical Heterojunction for Highly Sensitive Photodetectors. *ACS Appl. Mater. Interfaces* **2020**, *12*, 18769–18776. [CrossRef]
11. Guo, Z.; Zhang, J.; Liu, X.; Wang, L.; Xiong, L.; Huang, J. Optoelectronic Synapses and Photodetectors Based on Organic Semiconductor/Halide Perovskite Heterojunctions: Materials, Devices, and Applications. *Adv. Funct. Mater.* **2023**, *33*, 2305508. [CrossRef]
12. Cheng, X.; Han, Y.; Cui, B.-B. Fabrication Strategies and Optoelectronic Applications of Perovskite Heterostructures. *Adv. Opt. Mater.* **2022**, *10*, 2102224. [CrossRef]
13. Rathore, E.; Maji, K.; Rao, D.; Saha, B.; Biswas, K. Charge Transfer in the Heterostructure of CsPbBr3 Nanocrystals with Nitrogen-Doped Carbon Dots. *J. Phys. Chem. Lett.* **2020**, *11*, 8002–8007. [CrossRef]
14. DuBose, J.T.; Kamat, P.V. Efficacy of Perovskite Photocatalysis: Challenges to Overcome. *ACS Energy Lett.* **2022**, *7*, 1994–2011. [CrossRef]
15. Mahmood, A.; Shi, G.; Sun, J.; Liu, J. Investigation of electronic structure and optical properties of thallium lead halides: First principle calculations. *J. Appl. Phys.* **2018**, *124*, 093102. [CrossRef]
16. Odziomek, M.; Giusto, P.; Kossmann, J.; Tarakina, N.V.; Heske, J.; Rivadeneira, S.M.; Keil, W.; Schmidt, C.; Mazzanti, S.; Savateev, O.; et al. "Red Carbon": A Rediscovered Covalent Crystalline Semiconductor. *Adv. Mater.* **2022**, *34*, 2206405. [CrossRef]
17. Brodie, B.C., IV. On the action of electricity on gases.—II. On the electric decomposition of carbonic-acid gas. *Philos. Trans. R. Soc. Lond.* **1997**, *164*, 83–103. [CrossRef]
18. Ellern, A.; Drews, T.; Seppelt, K. The Structure of Carbon Suboxide, C_3O_2, in the Solid State. *Z. Anorg. Allg. Chem.* **2001**, *627*, 73–76. [CrossRef]
19. Smith, R.N.; Young, D.A.; Smith, E.N.; Carter, C.C. The Structure and Properties of Carbon Suboxide Polymer. *Inorg. Chem.* **1963**, *2*, 829–838. [CrossRef]
20. Giusto, P.; Cruz, D.; Rodriguez, Y.; Rothe, R.; Tarakina, N.V. Red Carbon Thin Film: A Carbon–Oxygen Semiconductor with Tunable Properties by Amine Vapors and Its Carbonization toward Carbon Thin Films. *Adv. Mater. Interfaces* **2022**, *9*, 2200834. [CrossRef]
21. Huang, H.; Verhaeghe, D.; Weng, B.; Ghosh, B.; Zhang, H.; Hofkens, J.; Steele, J.A.; Roeffaers, M.B.J. Metal Halide Perovskite Based Heterojunction Photocatalysts. *Angew. Chem. Int. Ed.* **2022**, *61*, e202203261. [CrossRef]
22. Oliveira, W.L.; de Oliveira, E.F.; do Carmo Batista, W.V.F.; Mourão, H.A.J.L.; Mendes Pires, M.J.; Coelho, R.M.; Atta Diab, G.A.; Teixeira, I.F.; Marques, G.; Mastelaro, V.R.; et al. A metal-free catalyst based on g-C_3N_4 functionalized with cyamelurate-like groups: Catalytic properties and mechanism of a new heterogeneous Fenton-like catalyst. *Carbon* **2023**, *214*, 118366. [CrossRef]
23. Oliveira, W.L.; Ferreira, M.A.; Mourão, H.A.J.L.; Pires, M.J.M.; Ferreira, V.; Gorgulho, H.F.; Cipriano, D.F.; Freitas, J.C.C.; Mastelaro, V.R.; Nascimento, O.R.; et al. Heterogeneous Fenton-like surface properties of oxygenated graphitic carbon nitride. *J. Colloid Interface Sci.* **2021**, *587*, 479–488. [CrossRef] [PubMed]
24. Ba, J.; Dong, H.; Odziomek, M.; Lai, F.; Wang, R.; Han, Y.; Shu, J.; Antonietti, M.; Liu, T.; Yang, W.; et al. Red Carbon Mediated Formation of Cu_2O Clusters Dispersed on the Oxocarbon Framework by Fehling's Route and their Use for the Nitrate Electroreduction in Acidic Conditions. *Adv. Mater.* **2024**, *36*, 2400396. [CrossRef]
25. Zheng, X.; Tian, Z.; Bouchal, R.; Antonietti, M.; López-Salas, N.; Odziomek, M. Tin (II) Chloride Salt Melts as Non-Innocent Solvents for the Synthesis of Low-Temperature Nanoporous Oxo-Carbons for Nitrate Electrochemical Hydrogenation. *Adv. Mater.* **2024**, *36*, 2311575. [CrossRef]

26. Akkerman, Q.A.; Manna, L. What Defines a Halide Perovskite? *ACS Energy Lett.* **2020**, *5*, 604–610. [CrossRef]
27. Araújo, T.C.; Oliveira, H.d.S.; Teles, J.J.S.; Fabris, J.D.; Oliveira, L.C.A.; de Mesquita, J.P. Hybrid heterostructures based on hematite and highly hydrophilic carbon dots with photocatalytic activity. *Appl. Catal. B Environ.* **2016**, *182*, 204–212. [CrossRef]
28. Lampman, G.M.; Pavia, D.L.; Kriz, G.S.; Vyvyan, J.R. *Introduçao a Espectroscopia*; Cengage: Boston, MA, USA, 2014.
29. Klug, H.P.; Alexander, L. The Crystal Structure of Ammonium Pentachlorozincate1. *J. Am. Chem. Soc.* **1944**, *66*, 1056–1064. [CrossRef]
30. Friese, K.; Madariaga, G.; Breczewski, T. Tricaesium Tetraiodozincate(II) Iodide, Cs3ZnI5. *Acta Crystallogr. Sect. C* **1998**, *54*, 1737–1739. [CrossRef]
31. Gaffar, M.A.; El-Fadl, A.A.; Anooz, S.B. Effects induced by chemical non-stoichiometry and γ-irradiation on the habit and unit cell parameters of ammonium tetrachlorozincate. *Cryst. Res. Technol.* **2006**, *41*, 379–387. [CrossRef]
32. Balasubramanian, M.; Ramakrishnan, V.; Rajendran, S. Vibrational spectra of $(NH_4)_3ZnCI_5$. *J. Phys.* **1991**, *36*, 8.
33. Yu, W.; Li, F.; Huang, T.; Li, W.; Wu, T. Go beyond the limit: Rationally designed mixed-dimensional perovskite/semiconductor heterostructures and their applications. *Innovation* **2023**, *4*, 100363. [CrossRef] [PubMed]
34. Tawil, C.A.; Kurdi, R.E.; Patra, D. Cesium Lead Bromide Perovskites: Synthesis, Stability, and Photoluminescence Quantum Yield Enhancement by Hexadecyltrimethylammonium Bromide Doping. *ACS Omega* **2022**, *7*, 20872–20880. [CrossRef] [PubMed]
35. Schötz, K.; Askar, A.M.; Peng, W.; Seeberger, D.; Gujar, T.P.; Thelakkat, M.; Köhler, A.; Huettner, S.; Bakr, O.M.; Shankar, K.; et al. Double peak emission in lead halide perovskites by self-absorption. *J. Mater. Chem. C* **2020**, *8*, 2289–2300. [CrossRef]
36. Yang, X.; Zhang, X.; Deng, J.; Chu, Z.; Jiang, Q.; Meng, J.; Wang, P.; Zhang, L.; Yin, Z.; You, J. Efficient green light-emitting diodes based on quasi-two-dimensional composition and phase engineered perovskite with surface passivation. *Nat. Commun.* **2018**, *9*, 570. [CrossRef]

Disclaimer/Publisher's Note: The statements, opinions and data contained in all publications are solely those of the individual author(s) and contributor(s) and not of MDPI and/or the editor(s). MDPI and/or the editor(s) disclaim responsibility for any injury to people or property resulting from any ideas, methods, instructions or products referred to in the content.